



**Beyond lowest order mean-field theory for light interacting with atom arrays**F. Robicheaux <sup>1,2,\*</sup> and Deepak A. Suresh <sup>1</sup><sup>1</sup>*Department of Physics and Astronomy, Purdue University, West Lafayette, Indiana 47907, USA*<sup>2</sup>*Purdue Quantum Science and Engineering Institute, Purdue University, West Lafayette, Indiana 47907, USA*

(Received 14 May 2021; accepted 26 July 2021; published 4 August 2021)

Results from higher order mean-field calculations of light interacting with atom arrays are presented for calculations of one- and two-time expectation values. The atoms are approximated as two levels and are fixed in space. Calculations were performed for mean-field approximations that include the expectation value of one operator (mean field), two operators (mean field 2), and three operators (mean field 3). For the one-time expectation values, we examined three different situations to understand the convergence with increasing order of mean field and some limitations of higher order mean-field approximations. As a representation of a two-time expectation value, we calculated the  $g^{(2)}(\tau)$  for a line of atoms illuminated by a perpendicular plane wave at several emission angles and two different intensities. For many cases, the mean field 2 will be sufficiently accurate to quantitatively predict the response of the atoms as measured by one-time expectation values. However, the mean-field-3 approximation will often be needed for two-time expectation values.

DOI: [10.1103/PhysRevA.104.023702](https://doi.org/10.1103/PhysRevA.104.023702)**I. INTRODUCTION**

Light interacting with many closely spaced atoms leads to several interesting and complex many-body effects. Typically, these effects arise when the spacing between atoms is of the order of the light's wavelength or smaller. Superradiance and subradiance [1–21] are classic effects whereby the collective interaction with the light field substantially slows (subradiance) or speeds up (superradiance) the rate that light is emitted from the atom cloud. In addition, the collective interactions between the atoms can lead to the shift in the resonance frequency [22–31] or can qualitatively change the scattering pattern from the atom cloud [21,30–39]. In recent years, several groups have studied the possibility to use this collective interaction for the manipulation of light [18,21,39–42]. One particularly promising system is for the atoms to be in a regular array [16–24,39–49] in order to decrease the dephasing from near-field atom-atom interactions, which leads to stronger collective effects and qualitatively new phenomena.

Calculations of light interacting with a group of atoms have tended to fall into two groups. If the number of atoms is small enough, full density matrix calculations are performed. These calculations can be thought of as being exact in the sense that the results are progressively more accurate as, for example,  $\delta t$  gets smaller and the number of included states gets larger. If there are a large number of atoms and many possible excitations, mean-field calculations are performed because the state space of the density matrix quickly becomes too large to solve on even the largest computers, much less the resources of the average researcher. Often, then, the time-dependent operator equations are approximated by

replacing two-atom expectation values with the product of one-atom expectation values [11,14,23,29,30,36,48–51]. This method, the mean-field approximation, has an inherent accuracy in the sense that for a given situation, the error cannot be reduced below a fixed, nonzero value by, for example, decreasing  $\delta t$ . The mean-field approximation should work well if there is not much correlation in the system. If the light intensity is low or if it is known that there is only one excitation in the system, then the linear approximation, where the pair operators are set to zero, can be used [4–8,18,19,24–26,31–35,37–43,52,53]. The strengths and weaknesses of these methods are fairly obvious. The density matrix calculations are accurate, but require inordinate time and memory as the number of atoms increases. The mean-field or linear approximations lose accuracy as the correlation between atoms increases, but can be applied to many atoms ( $10^3$  atoms are routine, and more than  $10^5$  atoms in one case [38]).

There are approximations with accuracy between that of the mean-field approximation and a density matrix treatment [54]. Reference [55] described a method they called generalized mean field, which includes higher order correlations, and explicitly derived the time-dependent operator equations that correctly include single and pair expectation values but approximate triple expectation values; below, we will call this the mean-field-2 (MF2) approximation. (Using this convention, the usual mean-field approximation is MF1.) The MF2 approximation should be more accurate than the MF1 approximation, but without the computational effort of a density matrix calculation, and has been used in several calculations [10,15,22,44,55–60]. However, it is substantially slower than the MF1 method. For  $N$  atoms, the number of operations for one time step is proportional to  $3^1 N^2$  for the MF1 approximation and is proportional to  $3^2 N^3$  for the MF2 approximation. The extra computational time and extra programming

\*robichf@purdue.edu

complexity explains why the MF2 approximation is rarely used in practice.

Even higher order mean-field approximations result from keeping larger products in the time-dependent operator equations. For example, the MF3 equations correctly include single, pair, and triple expectation values, but approximates quadruple expectation values. The number of operations for the MF3 approximation is proportional to  $3^3 N^4$ , which can be onerous but is much faster than evaluating the full density matrix.

Besides the expectation values of operators, two-time expectation values are often of interest [10,20,24,47,56,61,62]. For example, the  $g^{(2)}(\tau)$  function, given by Eq. (25), is the normalized intensity-intensity correlation of emitted light. In principle, this can be calculated using higher order mean-field approximations. Realizing this, we adapted the MF2 and MF3 approximations to the calculation of two-time expectation values. However, unlike the calculation of expectation values, the MF2 approximation often did not give accurate results for two-time expectation values. We found a complete breakdown of the approximation even for very low light intensities, where we expected the small number of excitations would lead to weak, if any, correlation. In one case, we decreased the intensity until there was less than  $10^{-5}$  total excitations and the MF2 approximation still failed. For  $g^{(2)}(\tau)$ , there can be a strong dependence on three or more atom correlations even for weak excitations.

Spurred by this failure of the MF2 method, we followed the spirit of the derivation in Ref. [55] to include expectation values of triple-atom operators and tested the resulting approximation in a variety of cases from expectation values in a nearly uncorrelated system to two-time expectation values in a correlated system. The tests were strict in the sense that we increased the order of the approximation from MF1 to MF2 to MF3 until convergence was obtained or we directly compared with the results from full density matrix calculations. We found that the MF3 method often gave accurate results even when the MF2 method completely fails (more than 100% error).

The paper is organized as follows: Section II presents the basic equations for approximating expectation values and two-time expectation values [e.g.,  $g^{(2)}(\tau)$ ], Sec. III contains results for three situations involving expectation values and one situation for two-time expectation values, and Sec. IV summarizes the results. Section A of the Appendices describes the method for reducing the order of operators and Sec. B describes the method for obtaining the initial conditions for two-time expectation values.

## II. BASIC THEORY

We are using an excitation scheme where the atomic structure is approximated as a two-level system. The atoms will be considered as fixed in space, which means we are ignoring the atom recoil.

### A. Master equation formalism

All of the equations will use a simplified notation to reduce the size of the resulting equations. For the  $n$ th atom, the

ground and excited states are  $|g_n\rangle$  and  $|e_n\rangle$ . The operators used below follow the definitions

$$\hat{e}_n \equiv |e_n\rangle\langle e_n|, \quad \hat{\sigma}_n^- \equiv |g_n\rangle\langle e_n|, \quad \hat{\sigma}_n^+ \equiv |e_n\rangle\langle g_n|. \quad (1)$$

The equation for the  $N$ -atom density matrix [61] can be written in the form

$$\begin{aligned} \frac{d\hat{\rho}}{dt} = & \sum_n \left[ \frac{1}{i\hbar} [H_n, \hat{\rho}] + \mathcal{L}_n(\hat{\rho}) \right] \\ & + \sum_n \sum'_m \left[ \frac{1}{i\hbar} [H_{nm}, \hat{\rho}] + \mathcal{L}_{nm}(\hat{\rho}) \right], \end{aligned} \quad (2)$$

where a prime on the sum means  $m \neq n$ , the  $H_n$  is the one-atom Hamiltonian that arises from an external laser interacting with each atom,  $\mathcal{L}_n$  is from one-atom decays of the Lindblad type, the  $H_{nm}$  is the two-atom Hamiltonian from the dipole-dipole interactions, and  $\mathcal{L}_{nm}$  are the two atom decays from the dipole-dipole interactions. For the two-level cases considered here, these operators are

$$H_n = \hbar \left( \frac{\Omega_n^+}{2} \hat{\sigma}_n^+ + \frac{\Omega_n^-}{2} \hat{\sigma}_n^- - \Delta_n \hat{e}_n \right), \quad (3)$$

$$\mathcal{L}_n(\hat{\rho}) = \frac{\Gamma}{2} (2\hat{\sigma}_n^- \hat{\rho} \hat{\sigma}_n^+ - \hat{e}_n \hat{\rho} - \hat{\rho} \hat{e}_n), \quad (4)$$

$$H_{nm} = \hbar \Omega_{nm} \hat{\sigma}_n^+ \hat{\sigma}_m^-, \quad (5)$$

$$\mathcal{L}_{nm} = \frac{\Gamma_{nm}}{2} (2\hat{\sigma}_n^- \hat{\rho} \hat{\sigma}_m^+ - \hat{\sigma}_m^+ \hat{\sigma}_n^- \hat{\rho} - \hat{\rho} \hat{\sigma}_m^+ \hat{\sigma}_n^-), \quad (6)$$

where  $\Delta_n$  is the detuning of the transition for atom  $n$ , the  $\Omega_n^+ = (\Omega_n^-)^*$  is the complex Rabi frequency at atom  $n$  (for plane wave light,  $\Omega_n^+ = \Omega \exp[i\vec{k} \cdot \vec{R}_n]$  where  $\vec{k}$  is the wave number and  $\vec{R}_n$  is the atom position). The two-atom parameters are defined for  $m \neq n$  as

$$\Gamma_{nm} = g(\vec{R}_{nm}) + g^*(\vec{R}_{nm}) = 2\text{Re}[g(\vec{R}_{nm})], \quad (7)$$

$$\Omega_{nm} = \frac{g(\vec{R}_{nm}) - g^*(\vec{R}_{nm})}{2i} = \text{Im}[g(\vec{R}_{nm})], \quad (8)$$

$$g(\vec{R}) = \frac{\Gamma}{2} \left[ h_0^{(1)}(s) + \frac{3\hat{R} \cdot \hat{d}^* \hat{R} \cdot \hat{d} - 1}{2} h_2^{(1)}(s) \right], \quad (9)$$

$$g_{nm}^\pm \equiv \pm i \Omega_{nm} + \frac{1}{2} \Gamma_{nm}, \quad (10)$$

with  $\hat{d}$  the dipole unit vector,  $s = kR$ ,  $\hat{R} = \vec{R}/R$ , and  $h_\ell^{(1)}(s)$  the outgoing spherical Hankel function of angular momentum  $\ell$ :  $h_0^{(1)}(s) = e^{is}/(is)$  and  $h_2^{(1)}(s) = (-3i/s^3 - 3/s^2 + i/s)e^{is}$ . The  $g(\vec{R})$  is proportional to the propagator that gives the electric field at  $\vec{R}$ , given a dipole at the origin [63]. For a  $\Delta M = 0$  transition,  $\hat{d} = \hat{z}$  and the coefficient of the  $h_2^{(1)}$  Bessel function is  $P_2[\cos(\theta)] = [3\cos^2(\theta) - 1]/2$ , where  $\cos(\theta) = Z/R$ . For a  $\Delta M = \pm 1$  transition, the coefficient of the  $h_2^{(1)}$  Bessel function is  $-(1/2)P_2[\cos(\theta)] = [1 - 3\cos^2(\theta)]/4$ .

### B. Operator equation formalism

The developments in this section are similar to those in Ref. [55] for including expectation values of two operators, with the exception that Ref. [55] uses the operators that give all real equations,  $\hat{\sigma}_{x,y,z}$ , whereas we use operators that lead to

complex equations,  $\hat{\sigma}^\pm$ . We have shown that our equations are the same as in Ref. [55], except for the typographical error in their Eq. (5 c) where the  $-i$  should be  $-1$ .

In order to make the notation more compact in this section, we will define the following:

$$\hat{Q}_n^{-1} = \hat{\sigma}_n^-, \quad \hat{Q}_n^0 = \hat{e}_n, \quad \hat{Q}_n^1 = \hat{\sigma}_n^+. \quad (11)$$

### 1. One-atom contributions

This section gives the contribution to the time dependence of the expectation value of operators due to the terms with  $H_j$  and  $\mathcal{L}_j$ . The equations of motion for the one-atom terms are

$$\frac{d\langle \hat{Q}_n^j \rangle}{dt} = \text{Tr} \left[ \hat{Q}_n^j \frac{d\hat{\rho}}{dt} \right] = S_n^j + \sum_{j'=-1}^1 W_n^{jj'} \langle \hat{Q}_n^{j'} \rangle, \quad (12)$$

where the second step results by replacing the derivative of the density matrix with the first line of the right-hand side of Eq. (2). Performing this substitution gives (counting rows and columns in order:  $-1, 0, 1$ )

$$\underline{W}_n = \begin{pmatrix} i\Delta_n - \frac{\Gamma}{2} & i\Omega_n^+ & 0 \\ i\frac{\Omega_n^-}{2} & -\Gamma & -i\frac{\Omega_n^+}{2} \\ 0 & -i\Omega_n^- & -i\Delta_n - \frac{\Gamma}{2} \end{pmatrix}, \quad (13)$$

$$\underline{S}_n = \begin{pmatrix} -i\frac{\Omega_n^+}{2} \\ 0 \\ i\frac{\Omega_n^-}{2} \end{pmatrix}. \quad (14)$$

Using this notation, the rate of change of the two-atom expectation values due to the one-atom terms in Eq. (2) can be found from Eq. (12), and are

$$\begin{aligned} \frac{d\langle \hat{Q}_n^j \hat{Q}_m^{j'} \rangle}{dt} &= S_n^j \langle \hat{Q}_m^{j'} \rangle + \langle \hat{Q}_n^j \rangle S_m^{j'} \\ &+ \sum_{j''=-1}^1 [W_n^{jj''} \langle \hat{Q}_n^{j''} \hat{Q}_m^{j'} \rangle + W_m^{j'j''} \langle \hat{Q}_n^j \hat{Q}_m^{j''} \rangle], \end{aligned} \quad (15)$$

where  $n \neq m$ .

The rate of change of the three and higher atom expectation values can be generalized from these equations.

### 2. Two-atom contributions

The two-atom contributions to the rate of change of the one-atom expectation values are

$$\frac{d\langle \hat{Q}_n^0 \rangle}{dt} = - \sum'_m (g_{nm}^+ \langle \hat{Q}_n^1 \hat{Q}_m^{-1} \rangle + g_{nm}^- \langle \hat{Q}_n^{-1} \hat{Q}_m^1 \rangle), \quad (16)$$

$$\frac{d\langle \hat{Q}_n^{\pm 1} \rangle}{dt} = \sum'_m g_{nm}^\mp (2\langle \hat{Q}_n^0 \hat{Q}_m^{\pm 1} \rangle - \langle \hat{Q}_m^{\pm 1} \rangle), \quad (17)$$

where a prime on the sum means  $m \neq n$  and  $g_{nm}^\pm$  are defined by Eq. (10). These equations can be generalized to the form

$$\frac{d\langle \hat{Q}_n^j \rangle}{dt} = \sum'_{j'm} V_{nm}^{jj'} \langle \hat{Q}_m^{j'} \rangle + \sum'_{j'j''m} U_{nm}^{jj'j''} \langle \hat{Q}_n^{j'} \hat{Q}_m^{j''} \rangle, \quad (18)$$

where a prime on the sum means  $m \neq n$  and the only nonzero elements are

$$V_{nm}^{\pm 1, \pm 1} = -g_{nm}^\mp, \quad (19)$$

$$U_{nm}^{0, \pm 1, \mp 1} = -g_{nm}^\pm, \quad U_{nm}^{\pm 1, 0, \pm 1} = 2g_{nm}^\mp. \quad (20)$$

In the two-atom expectation values, there are terms involving  $H_{nm}$  and  $\mathcal{L}_{nm}$  and there are terms involving  $nl$  and  $ml$  subscripts, where  $l \neq n$  and  $l \neq m$ . The latter terms can be found from application of Eqs. (16). This will lead to three operator expectation values in the expressions for the rate. These equations are

$$\begin{aligned} \frac{d\langle \hat{Q}_n^j \hat{Q}_m^{j'} \rangle}{dt} &= \sum'_{j'l} [V_{nl}^{jj'} \langle \hat{Q}_l^{j'} \hat{Q}_m^{j'} \rangle + V_{ml}^{jj'} \langle \hat{Q}_n^j \hat{Q}_l^{j'} \rangle] \\ &+ \sum'_{j''j'''l} U_{nl}^{jj''j'''} \langle \hat{Q}_n^{j''} \hat{Q}_l^{j'''} \hat{Q}_m^{j'} \rangle \\ &+ \sum'_{j''j'''l} U_{ml}^{jj''j'''} \langle \hat{Q}_n^j \hat{Q}_m^{j''} \hat{Q}_l^{j'''} \rangle, \end{aligned} \quad (21)$$

where  $m \neq n$  and a prime on the sum means  $l \neq m, n$ . The only nonzero contributions from  $H_{nm}$  and  $\mathcal{L}_{nm}$  that do not lead to connections with atoms  $l \neq m, n$  are

$$\frac{d\langle \hat{Q}_n^{-1} \hat{Q}_m^{+1} \rangle}{dt} = 2\Gamma_{nm} \langle \hat{Q}_n^0 \hat{Q}_m^0 \rangle - g_{nm}^+ \langle \hat{Q}_m^0 \rangle - g_{nm}^- \langle \hat{Q}_n^0 \rangle, \quad (22)$$

$$\frac{d\langle \hat{Q}_n^0 \hat{Q}_m^{\pm 1} \rangle}{dt} = -g_{nm}^\pm \langle \hat{Q}_n^{\pm 1} \hat{Q}_m^0 \rangle, \quad (23)$$

where the  $\Gamma_{nm}$  are defined in Eq. (7).

As an example that includes both types of terms, the two-atom contributions give

$$\begin{aligned} \frac{d\langle \hat{\sigma}_m^+ \hat{\sigma}_n^- \rangle}{dt} &= 2\Gamma_{mn} \langle \hat{e}_m \hat{e}_n \rangle - g_{nm}^+ \langle \hat{e}_m \rangle - g_{nm}^- \langle \hat{e}_n \rangle \\ &+ \sum'_l g_{nl}^+ (2\hat{e}_n \hat{\sigma}_l^- \hat{\sigma}_m^+ - \hat{\sigma}_l^- \hat{\sigma}_m^+) \\ &+ \sum'_l g_{ml}^- (2\hat{e}_m \hat{\sigma}_l^+ \hat{\sigma}_n^- - \hat{\sigma}_l^+ \hat{\sigma}_n^-), \end{aligned} \quad (24)$$

where the first line is from Eq. (22) and the terms in the sum are from Eq. (17) applied to the  $\hat{\sigma}_n^-$  and  $\hat{\sigma}_m^+$  operators.

The rate of change for three operator expectation values can be generated from these equations.

### C. Two-time correlation functions

In many situations, the calculation of two-time correlation functions can lead to useful information about the system, for example, the correlation in emitted photons. As an example, consider the combination

$$g^{(2)}(\tau) = \lim_{t \rightarrow \infty} \frac{\langle \hat{\sigma}^+(t) \hat{\sigma}^+(t+\tau) \hat{\sigma}^-(t+\tau) \hat{\sigma}^-(t) \rangle}{[\langle \hat{\sigma}^+ \hat{\sigma}^- \rangle(t)]^2}, \quad (25)$$

where

$$\hat{\sigma}^- = \sum_l e^{-i\vec{k} \cdot \vec{R}_l} \hat{\sigma}_l^- = \hat{\sigma}^{+\dagger}, \quad (26)$$

which is the normalized intensity-intensity correlations of light emitted in the  $\hat{k}$  direction. The denominator in Eq. (25) can be approximately calculated within the operator method described above. However, calculating the numerator requires an extension of the method.

The two-time correlations can be computed from the expectation value of operators using an algorithm based on a method for calculating the two-time expectation values from density matrices. For this discussion, we will use the example in Eq. (25) for the two-time expectation value. There are three steps in the calculation. Step (1): First calculate the density matrix using Eq. (2) up to time  $t$ . Step (2): At this time, a projected density matrix is calculated using

$$\frac{\hat{\sigma}^- \hat{\rho}(t) \hat{\sigma}^+}{\langle \hat{\sigma}^+ \hat{\sigma}^- \rangle(t)} \rightarrow \hat{\rho}(t). \quad (27)$$

Step (3): The density matrix equation, given by Eq. (2), is used to propagate to time  $t + \tau$ . Finally, the two-time expectation value is given by

$$\frac{\langle \hat{\sigma}^+(t) \hat{\sigma}^+(t + \tau) \hat{\sigma}^-(t + \tau) \hat{\sigma}^-(t) \rangle}{[\langle \hat{\sigma}^+ \hat{\sigma}^- \rangle(t)]^2} = \frac{\text{Tr}[\hat{\sigma}^+ \hat{\sigma}^- \hat{\rho}(t + \tau)]}{\langle \hat{\sigma}^+ \hat{\sigma}^- \rangle(t)}. \quad (28)$$

The operator method can be used within this scenario by tracking the effect of the different steps. Since some of the equations are long and complicated, Appendix B contains the derivations and the specific equations for both MF2 and MF3 calculations.

Step (1) is the same as usual, where the various coupled operator equations are solved as a function of time. The expectation value is given by Eq. (B3) and is

$$\langle \hat{\sigma}^+ \hat{\sigma}^- \rangle(t) = \sum_n \left[ \langle \hat{e}_n \rangle(t) + \sum'_m e^{i\varphi_{mn}} \langle \hat{\sigma}_m^+ \hat{\sigma}_n^- \rangle(t) \right], \quad (29)$$

where  $\varphi_{mn} = \vec{k} \cdot (\vec{R}_m - \vec{R}_n)$  and the prime on the sum means  $m \neq n$ .

Step (2) does not change the trace of the density matrix *but* the expectation values change. The expectation values after the transformation, given by Eq. (27), can be found from the new density matrix. The parts arising from the numerator,  $\hat{\sigma}^- \hat{\rho}(t) \hat{\sigma}^+$ , are in Appendix B.

Step (3) is the same as Step (1), but using the initial conditions from Step (2). At the time  $t + \tau$ , the expectation value  $\langle \hat{\sigma}^+ \hat{\sigma}^- \rangle$  is evaluated and is divided by the old value,  $\langle \hat{\sigma}^+ \hat{\sigma}^- \rangle(t)$ , to obtain  $g^{(2)}(\tau)$ .

#### D. Restricting correlations

The two-atom contributions to the operator equations lead to an increasing number of terms in the operator correlations: the time derivative of the one-atom expectation values depends on two-atom expectation values, the time derivative of two-atom expectation values depend on three-atom expectation values, etc. The set of equations only closes when the number of operators in the expectation values equals the number of atoms.

The set of equations can be closed by using approximations for the higher order expectation values. As described in Appendix A, we obtain the equations by setting the cumulant [64] at a given order to zero, as done in

Refs. [10,15,22,44,55–60]. For example, the mean-field (MF1) approximation results from using the approximation of Eq. (A6) to replace a two-atom expectation value by the product of one-atom expectation values as

$$\langle \hat{Q}_n^i \hat{Q}_m^{j'} \rangle \leftarrow \langle \hat{Q}_n^i \rangle \langle \hat{Q}_m^{j'} \rangle. \quad (30)$$

Typically, a better approximation results from keeping the two-atom expectation values but replacing the three-atom expectation values by their cumulant approximation, given by Eq. (A7), to give

$$\begin{aligned} \langle \hat{Q}_n^i \hat{Q}_m^{j'} \hat{Q}_l^{j''} \rangle &\leftarrow \langle \hat{Q}_n^i \hat{Q}_m^{j'} \rangle \langle \hat{Q}_l^{j''} \rangle + \langle \hat{Q}_n^i \hat{Q}_l^{j''} \rangle \langle \hat{Q}_m^{j'} \rangle \\ &+ \langle \hat{Q}_n^i \rangle \langle \hat{Q}_m^{j'} \hat{Q}_l^{j''} \rangle - 2 \langle \hat{Q}_n^i \rangle \langle \hat{Q}_m^{j'} \rangle \langle \hat{Q}_l^{j''} \rangle. \end{aligned} \quad (31)$$

Below, MF2 calculations are those where this replacement has been made.

An even better approximation typically results from keeping the two and three operator expectation values, but approximating the four operator expectation values using the replacement in Eq. (A8). Below, MF3 calculations are those where this replacement has been made.

This process can be continued to even higher order products, which are typically more accurate than those of lower order. In principle, going to higher order is a systematic way for increasing the accuracy of a calculation. However, the speed of the resulting programs rapidly decreases with the order kept.

### III. RESULTS

In this section, we will refer to calculations that use Eq. (30) as mean-field or MF1 calculations, those that use Eq. (31) as MF2 calculations, and those that use Eq. (A8) as MF3 calculations.

#### A. One-time expectation values

This section describes results from three types of calculations that compare the different order mean-field calculations with that from a full density matrix treatment. The topics are presented in order from least correlated to most correlated.

##### 1. Collective shift in a line of atoms

We use the operator formalism to calculate an observable from Ref. [30]. In Ref. [30], they measured the collective shift in scattered light from a one-dimensional chain of atoms. They also performed calculations using the MF1 approximation, equivalent to using Eq. (30), to interpret their results. For the most part, there was good agreement between this approximation and the measurements, except for their Fig. 4(a) for the global resonance shift versus the driving amplitude,  $\Omega/\Gamma$ . In this situation, they showed the detuning versus the Rabi frequency and experimentally found a steep drop in the shift at  $\Omega \sim 1.5\Gamma$ , whereas the calculation showed a smooth decrease with increasing Rabi frequency. They presented the comparison between a full density matrix calculation and the MF1 approximation for six atoms which showed good agreement; this agreement suggests that the mean-field approximation itself was not the source of the disagreement. However, it is not completely clear whether or not the MF1 approximation

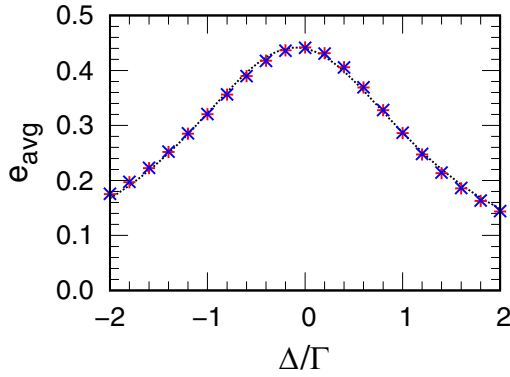


FIG. 1. The average excitation probability for 100 atoms in the configuration of Ref. [30] for  $\Omega = 2\Gamma$ . The red \* are from a MF1 calculation, while the blue  $\times$  are from a MF2 calculation. The black dotted line is a Lorentzian fit to the MF2 points.

could fail at larger  $N$  because the atoms are roughly in a line. We performed calculations with many more atoms at both the MF1 and MF2 level as a test of the accuracy of the mean-field approximation.

We constructed the simulation to mimic as many aspects of the experiment as possible. The atoms are trapped using a Gaussian standing wave with, on average, a 50% probability for an atom at each intensity maximum. The atoms are mainly along the  $z$  axis and are excited with an  $M = 1$  transition. The atoms have a Gaussian distribution in  $x, y$  with a transverse width  $\sigma_\rho = 300$  nm. The Gaussian beam has wavelength of 940 nm and waist of  $3.3 \mu\text{m}$ , giving a Rayleigh range  $Z_R = 36.4 \mu\text{m}$ . The  $z$  position of the atoms is found from the zeros of  $\sin[kz - \arctan(z/Z_R)]$ , with  $k = 2\pi/(940 \text{ nm})$ . Since the detector is perpendicular to the line of atoms, the measured light scattered is proportional to  $\sum_n \langle \hat{e}_n \rangle$ .

Figure 1 shows results from a calculation with 100 atoms averaged over 200 configurations of atom positions for  $\Omega = 2\Gamma$ , where the experiment has  $\sim 0$  detuning. The red \* are from MF1 calculations, while the blue  $\times$  are from a MF2 calculation. This is an ideal application of the higher order mean-field calculations result because we could increase the order until the results agree. The black dotted line is a Lorentzian fit to the MF2 points. The fit gave a collective shift of  $-0.093\Gamma$ , which is in line with the calculation in Ref. [30] but in disagreement with the measurements. Thus, the MF1 approximation is not the cause for disagreement in this experiment.

## 2. Normal mode excitation

As another example, we explore the case presented in Ref. [48] where a line of seven atoms is excited with circularly polarized light. We present results for the case where the atoms are separated by  $0.4\lambda$ . Following Ref. [48], the atoms are excited with amplitudes taken from the eigenvectors,  $u_\alpha(\vec{R}_n)$ , of the complex symmetric,  $g_{mn}^+ : \sum_n g_{mn}^+ u_\alpha(\vec{R}_n) = G_\alpha u_\alpha(\vec{R}_m)$  with the normalization  $\sum_n |u_\alpha(\vec{R}_n)|^2 = 1$  [65]. To organize the states, we use the decay rate of the eigenstate,  $2\text{Re}[G_\alpha]$ ; and  $\Omega_n^+ = \Omega u_\alpha(\vec{R}_m)$ . As with Ref. [48], we compute

the rate of scattered photons as

$$\gamma = \sum_n \left[ \Gamma \langle \hat{e}_n \rangle + \sum'_m \Gamma_{mn} \langle \hat{\sigma}_m^+ \hat{\sigma}_n^- \rangle \right], \quad (32)$$

$$\gamma_C = \sum_n \left[ \Gamma \langle \hat{\sigma}_n^+ \rangle \langle \hat{\sigma}_n^- \rangle + \sum'_m \Gamma_{mn} \langle \hat{\sigma}_m^+ \rangle \langle \hat{\sigma}_n^- \rangle \right], \quad (33)$$

$$\gamma_I = \gamma - \gamma_C, \quad (34)$$

where  $\Gamma_{mn}$  is from Eq. (7) and a prime on the sum indicates  $m \neq n$ . The  $\gamma$  is the total scattering rate, the  $\gamma_C$  is the classical approximation to the scattering rate, and the  $\gamma_I$  is the incoherent scattering rate.

As with Ref. [48], we calculate  $\delta\gamma_C \equiv (\gamma_C^{\text{lin}} - \gamma_C)/\gamma_C$  and the  $\gamma_I/\gamma_C$  for the different eigenstates. The  $\gamma_C^{\text{lin}}$  uses the linear approximation to the operator equations; this is equivalent to using Eq. (30) with the additional approximation  $\langle \hat{e}_n \rangle(t) = 0$ . For the intensities investigated, the  $\gamma_C^{\text{lin}} \sim \gamma_C$ , which means the  $\delta\gamma_C$  strongly emphasizes any error in the approximation.

Figure 2 shows plots versus the incident intensity in units of the saturation intensity,  $I_{in}/I_s \equiv 2\Omega^2/\Gamma^2$ , comparing the density matrix results (lines in all figures) to those using the MF1 approximation [Fig. 2(a) and red + in Fig. 2(c)] and MF2 approximation [Fig. 2(b) and blue  $\times$  in Fig. 2(c)]. The MF3 approximation is only plotted in Fig. 2(c) (orange \*) because the MF2 is already in agreement for the other cases.

As noted in Ref. [48], the MF1 approximation, given by Eq. (30), in Fig. 2(a) and red + in Fig. 2(c), has a qualitative relationship with the density matrix result. This level of approximation does not even give the correct order to the curves: the purple solid and green hollow squares are reversed. However, the MF2 approximation, given by Eq. (31), provides quantitative agreement with the density matrix result, except for the most subradiant state in Fig. 2(c). This is in agreement with the finding in Ref. [55] that the second order correlations greatly improve the agreement with the full density matrix result. Lastly, the MF3 approximation, given by Eq. (A8), provides quantitative agreement for all of the curves; this is shown in Fig. 2(c) where this approximation, i.e., the orange \*, is on top of the red line for all intensities. To give an idea of the accuracy, the value for the largest intensity of the most subradiant state has an error of 18%, 5.0%, and 0.18% for the MF1, MF2, and MF3 approximations, respectively.

This is nearly an ideal application of the higher order mean-field calculations result because we could increase the order until the results agree for all but one of the cases. While the convergence with increasing order for the most subradiant case would lead to the expectation that the MF3 result was accurate, it would be difficult to quantify that accuracy without knowing the result from the exact, density matrix calculation.

## 3. Collective decay from the totally excited state

The last example in this section is the case where there is no laser causing stimulated absorption or emission and all atoms start in the excited state [1]. This is the case treated by Dicke with the approximation of  $\Omega_{mn} = 0$ ,  $\Gamma_{mn} = \Gamma$  and can lead to superradiance or subradiance depending on the circumstances. For our calculations, we will use the correct

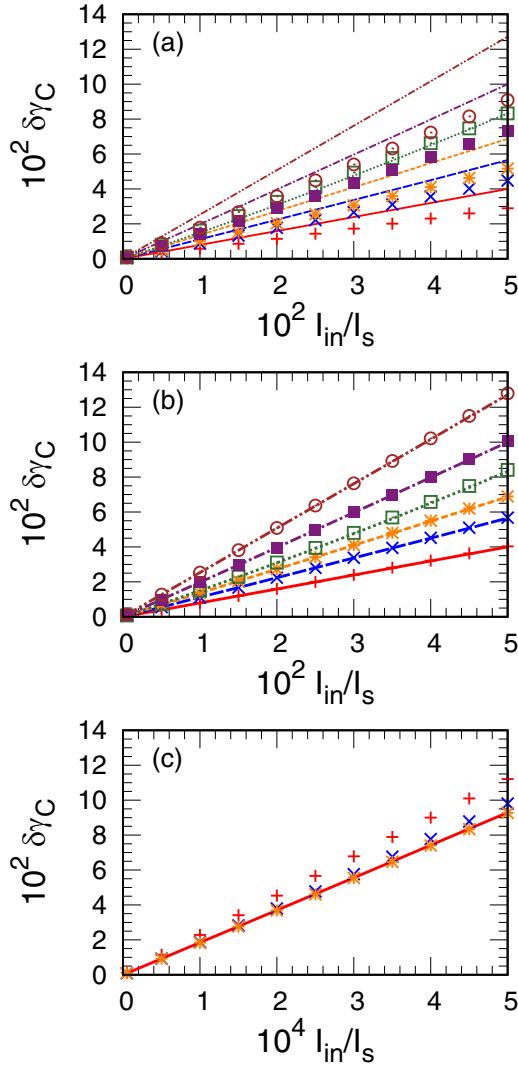


FIG. 2. The  $\delta\gamma_C$  for the case of seven equally spaced atoms,  $\Delta z = 0.4\lambda$ , excited to the different eigenmodes of light traveling along  $z$  with circular polarization. The  $I_{in}/I_s = \Omega^2/(2\Gamma^2)$ . In (a) and (b), the decay rate of the eigenstate,  $2\text{Re}[G_\alpha]$ , corresponding to each line in increasing order (solid red to dot-dash-dashed brown) is 1.413, 1.294, 1.147, 0.975, 1.032, and 0.961 times the one-atom decay rate  $\Gamma$ . The decay rate for (c) is 0.179 times  $\Gamma$ . In all cases, the lines are from solving the full density matrix equations. The symbols in (a) are from the calculation using the approximation in Eq. (30), while those in (b) are from Eq. (31). In both cases, the color matches that of the corresponding line (in order: red +, blue  $\times$ , orange \*, green hollow square, purple filled square, brown hollow circle). In (c), the red + is from MF1, given by Eq. (30), the blue  $\times$  are from MF2, given by Eq. (31), and the orange \* are from MF3, given by Eq. (A8).

forms of  $\Omega_{mn}$  and  $\Gamma_{mn}$ . Note that the MF1 equations lead to the solution  $\langle \hat{e}_n \rangle(t) = \exp(-\Gamma t)$  and  $\langle \hat{\sigma}_n^\pm \rangle(t) = 0$ , which does not contain any multiatom effects.

For this calculation, we reproduce the case discussed in Ref. [20] where atoms are equally spaced on a line. Figure 3 shows the photon emission rate for eight atoms in a line with separation  $\Delta z = 0.1\lambda$ , where the states make  $M = 1$  transitions. Plotted are the emission rate for the density matrix equations (red solid line), for the MF2 equations (blue

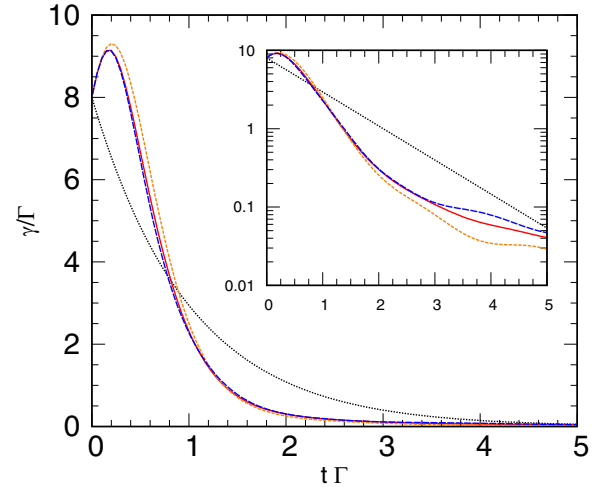


FIG. 3. The instantaneous decay rate  $\gamma$ , given by Eq. (32), for eight equally spaced atoms with a separation:  $\Delta z = 0.1\lambda$ . The states only support  $M = 1$  transitions. The red solid line is from solving the density matrix equations. The orange short-dashed line is from solving the operator equations at the MF2 level, given by Eq. (31), and the dashed blue line is at the MF3 level, given by Eq. (A8). The black dotted line is  $8e^{-\Gamma t}$  and is the MF1 solution. The inset is the same plot, but with a logarithmic scale for the y axis.

dashed line), for the MF3 approximation (orange short-dashed line), and the MF1 results (black dotted line) which have no multiatom effects. The early time increase in the photon emission rate is due to superradiance of this system, which is a collective effect. The MF1 calculation cannot reproduce any aspect of the collective decay. The MF2 approximation reproduces many aspects of the time-dependent decay rate when the decay rate is large. In contrast, the MF3 approximation is in quantitative agreement with the exact result when the decay rate is at least  $\sim 1\%$  of the peak decay rate. At longer times and smaller decay rates, none of the approximations are quantitatively accurate, as seen in the inset. This is during part of the time evolution where subradiant states are the largest component of the signal, indicating that the mean-field approximations are not accurately populating these states.

This is the worst case for one-time expectation values. The MF1 calculation is not even qualitatively accurate, missing all of the important physics. The MF2 and MF3 approximations decently agree with each other where  $\gamma$  is large. For this region, one would expect that the MF3 calculation is accurate. However, for later times, the MF2 and MF3 calculations differ by a factor of  $\sim 2$  and, thus, one would not have any expectation for the level of accuracy of the MF3. In fact, there are regions of substantial disagreement with the exact density matrix results, indicating that the subradiant states are not accurately populated by the MF3 equations at late times.

## B. Two-time expectation values

This section contains results from two-time expectation values. In particular, we will examine how well the mean-field approximations reproduce the  $g^{(2)}(\tau)$  function in Eq. (25) when the atoms are uniformly excited as would happen in an experiment where atoms are excited by a plane wave. We

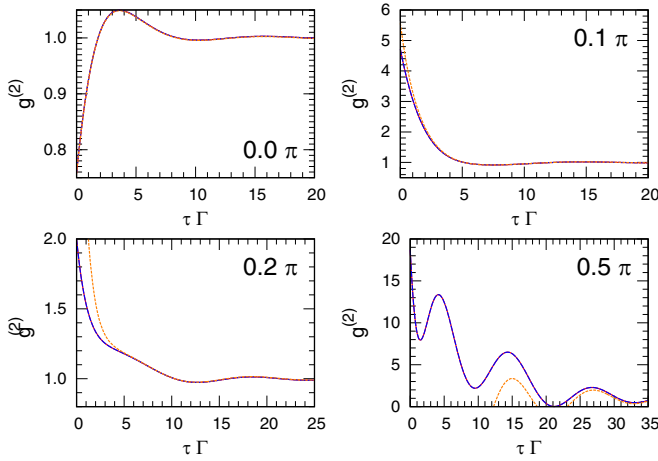


FIG. 4. The  $g^{(2)}(\tau)$  from Eq. (25) for seven atoms spaced by  $0.4\lambda$  on the  $y$  axis with plane wave light incident from the  $x$  direction. The atoms are linearly polarized in the  $z$  direction and the  $\Omega_n = \Gamma/100$ . The solid red line is from a density matrix calculation, the short-dashed orange line is from a MF2 calculation, and the dashed blue line is from a MF3 calculation. The calculations are for final photon angles of  $0.0, 0.1, 0.2$ , and  $0.5\pi$  relative to the  $x$  axis in the  $xy$  plane.

find that this is a more difficult test than calculating one-time expectation values. For the cases we tested, the MF1 result never gave an interesting result so we will only show the calculations using the MF2 and MF3 approximations.

All of the calculations in this section are for seven atoms in a line separated by  $0.4\lambda$  on the  $y$  axis. The incident light is propagating perpendicular to the line of atoms in the  $x$  direction. Thus, the  $\Omega_n$  are identical. The atoms are linearly polarized in the  $z$  direction. We present results for  $g^{(2)}(\tau)$  for different  $\hat{k}$  in the  $xy$  plane. The angle  $\theta$  is the final direction of the photons relative to the  $x$  axis. The direction  $\theta = 0$  has the most scattered photons and there is a rapid drop in scattering probability as  $\theta$  increases. In all of the plots, the solid red line is from a density matrix calculation, the short-dashed orange line is from a MF2 calculation, and the dashed blue line is from a MF3 calculation.

Figure 4 shows results for  $g^{(2)}(\tau)$  for  $\Omega_n = \Gamma/100$ . The one-time average  $\langle \hat{\sigma}^+ \hat{\sigma}^- \rangle(t)$  from Eq. (29) at large time is proportional to the rate of photons scattered into that direction. We did calculations of this expectation value at angles from  $0.0$  to  $0.5\pi$  in steps of  $0.1\pi$  and found values of  $(3.11 \times 10^{-3}, 1.08 \times 10^{-3}, 1.38 \times 10^{-4}, 5.88 \times 10^{-5}, 5.84 \times 10^{-5}, 3.20 \times 10^{-5})$ , which shows the drop in photon scattering with angle. Both the MF2 and MF3 calculations of these values were accurate, with the MF2 error less than  $0.1\%$  at  $0.0\pi$ , increasing to  $2\%$  error at  $0.5\pi$ , while the MF3 approximation was accurate to at least seven significant digits for all angles. The  $g^{(2)}(\tau)$  has antibunching behavior for scattering into  $0.0\pi$  with  $g^{(2)}(0) < 1$ , but has bunching behavior,  $g^{(2)}(0) > 1$ , for the larger angles that are calculated. For photon scattering along the atom line  $0.5\pi$ , the  $g^{(2)}(0) \simeq 19$ .

The MF3 calculations reproduce the density matrix calculations for all angles, even for larger angles where few photons are scattered and where there is a strong correlation between

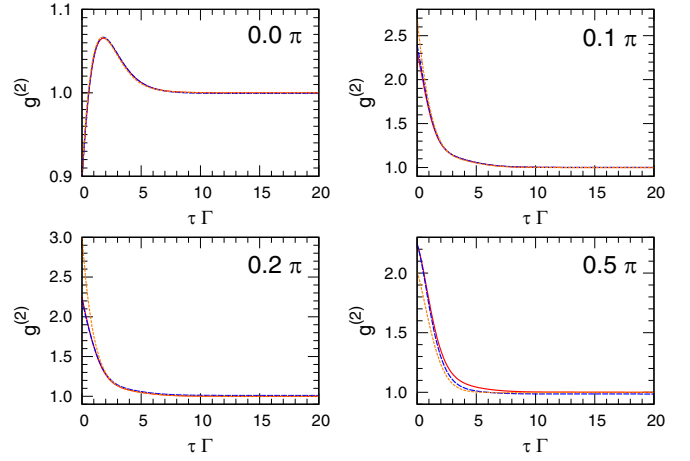


FIG. 5. Same as Fig. 4, but for  $\Omega_n = \Gamma/2$ .

successive photons. This is not surprising because the  $\Omega_n$  are small, and the expectation values decrease rapidly with increasing number of operators in the expectation value. The MF2 calculation reproduces the density matrix calculation for  $0.0\pi$  and is in decent agreement for  $0.1\pi$ . However, at  $0.2\pi$ , the  $g^{(2)}(0)$  is too large by a factor of  $\simeq 2.3$ , and for larger angles, the error is even larger. Worse, the MF2 calculation is negative for  $0.4$  and  $0.5\pi$ , which is unphysical. This is, perhaps, surprising because  $\Omega$  is small and an argument similar to that for MF3 can be made. Perhaps more interestingly, the MF2 approximation does not increase in accuracy for the larger angles as  $\Omega$  is decreased, which violates the expectation that there should be less correlation for smaller excitation probabilities: calculations with  $\Omega = 10^{-5}\Gamma$  had similar size errors to those in Fig. 4. The difficulty is to get the correct value for  $g^{(2)}(0)$ . This incorrect initial value means that the starting conditions for the one- and two-atom operators are not accurate. The problem appears to be with the  $\langle \hat{\sigma}_m^+ \hat{\sigma}_l^- \rangle(t=0)$  terms, which are of the same size as the  $\langle \hat{\sigma}_l \rangle(t=0)$ . The starting two operator terms are evaluated from Eq. (B9), which has three and four operator expectation values that are important. These expectation values are not included in the MF2 equations and must be approximated from the cumulant relation.

Figure 5 shows the same results for  $\Omega_n = \Gamma/2$ . For this case, the one-time average  $\langle \hat{\sigma}^+ \hat{\sigma}^- \rangle(t)$  from Eq. (29) at large time is  $4.55, 0.480, 0.505, 0.389, 0.431, \text{ and } 0.452$  for the angles from  $0.0$  to  $0.5\pi$ . The MF2 had  $1\%$  error at  $0.0\pi$ , increasing to  $6\%$  error at  $0.5\pi$ , while the MF3 had less than  $0.01\%$  error at  $0.0\pi$  and  $1\%$  error at  $0.5\pi$ . The  $g^{(2)}(\tau)$  again shows antibunching behavior for  $0.0\pi$ , but bunching for larger angles. Unlike the previous weak laser case, the  $g^{(2)}(\tau)$  does not achieve very large values for the larger angles. This is due to the higher intensity leading to more excitation and less suppression of photon scattering into the higher angles. Also unlike the previous case, the MF2 does not have qualitative errors, which indicates there is less correlation. The MF3 does have visible errors for the larger angles, indicating the start of the breakdown of this approximation, but the errors are small.

A more interesting aspect of the breakdown was that the  $g^{(2)}(\tau)$  did not go to  $1$  at large  $\tau$  for MF3. This indicates that the errors are large enough to trap the nonlinear MF3

equations in unphysical parameter regions for the expectation values. We examined the  $\langle \hat{e}_l \hat{e}_m \rangle$  after doing the projection step, given by Eq. (27). For the weak laser case,  $\Omega_n = \Gamma/100$ . Both mean-field approximations had instances of negative values, which is not physical, but the MF3 was much smaller. For MF3, the negative values were  $\sim 100\times$  smaller in magnitude than the largest positive values, while the negative values were only  $\sim 5\times$  smaller for MF2. There were no negative values for the  $\Omega_n = \Gamma/2$  example because there is relatively more photon scattering into the larger angles. This breakdown is a reminder that physical constraints are not necessarily obeyed in the mean-field approximations.

This case shows that it will often be difficult to show convergence of the mean-field equations with increasing order for the two-time expectation values. Although the MF3 was in good agreement with the density matrix results for all cases, some external test of convergence may be necessary. This external test might be a comparison with experiment or a comparison with density matrix results for a smaller number of atoms.

### C. Unphysical behavior

The previous section had examples where the MF2 and MF3 results were not just incorrect, but were unphysical for some parameters. In other situations, it was found that the higher order mean-field equations were unstable [66,67], which was not the case for any of the examples we investigated. It could be that the damping given by Eq. (2) helps stabilize the higher order mean-field cases we investigated. Another possibility is that the atomic arrays prevent large values of  $g_{nm}^\pm$  that occur with randomly placed atoms; perhaps large  $g_{nm}^\pm$  could lead to instability. If instabilities occur, they would be due to the inherent inaccuracy of the equations and could not be fixed by, for example, using smaller  $\delta t$  when solving the coupled equations.

## IV. SUMMARY

Higher order mean-field calculations of both one- and two-time expectation values were calculated for the interaction of light with two-level atoms in four different situations. For the one-time expectation values, we have repeated the derivation of Ref. [55], but for the complex expectation values from  $\hat{\sigma}^\pm$  instead of the real expectation values from the Pauli spinors. As higher order expectation values are included, the mean-field method becomes more accurate but more difficult to implement. We have also derived the equations needed to compute the two-time expectation values, for example,  $g^{(2)}(\tau)$ . We found the two-time expectation values to be less accurate than one-time expectation values for a given mean-field order. The calculations also highlight the difficulty, in some cases, of proving convergence by increasing the order of the mean-field equations.

The one-time expectation values were most easily reproduced using the higher order mean-field approximations. The first case addressed was the experiment of Ref. [30], which measured the shift in the scattering of light from a line of atoms. The MF1 and MF2 results were nearly identical. The next case was based on Ref. [48], which examined the scatter-

ing of light from a line of atoms when the excitation pattern was an eigenmode of the interaction. While the MF1 results were in qualitative agreement with exact calculations, the MF2 and MF3 results were in better agreement so that the error was less than 0.2% for all cases at the MF3 level. The last case was the collective decay from a line of atoms that starts with all atoms excited. The MF1 result was not even in qualitative agreement; it could not account for even the basic physics. The MF2 was in decent agreement when the photon emission rate was large and the MF3 was in excellent agreement in this range. However, at later times, the MF2 was more than a factor of 2 off while the MF3 was in rough agreement, indicating that neither approximation was accurate with regards to the population of subradiant states at late times.

The two-time expectation values were represented by calculations of  $g^{(2)}(\tau)$  for a line of atoms excited by a plane wave. The MF1 results were qualitatively incorrect. For the angles where the majority of photons were scattered, the MF2 and MF3 approximations reproduced the time dependence of  $g^{(2)}(\tau)$ . However, at angles where few photons were scattered, the MF2 calculation was not even in qualitative agreement and, in some cases, had strongly unphysical features. The MF3 approximation was in excellent agreement for weak light and in good agreement for stronger excitation in the cases tested. In some cases, an external method for estimating the accuracy of the mean-field method will be needed.

Overall, it appears that the MF2 approximation will often be accurate for calculations of one-time expectation values. However, for many two-time expectation values, the MF3 approximation will be needed.

Recently, we became aware of Ref. [68], which describes a computational toolbox for the cases discussed in our paper as well as extensions for cavities and mechanical oscillation of a membrane.

## ACKNOWLEDGMENTS

We thank J. Ruostekoski and L.A. Williamson for helping us understand Ref. [48]. This work was supported by the National Science Foundation under Grant No. 1804026-PHY.

## APPENDIX A: REDUCTION OF OPERATOR EXPECTATION VALUES

This section contains the algorithm used to reduce higher order expectation values to lower order.

### 1. Cumulants for 2 through 5 operators

The operator equations do not close until the number of operators equals the number of atoms. To obtain useful equations when the number of operators is much less than the number of atoms, a method for approximating a higher order product of operators by those with smaller products must be chosen. The results presented here use a cumulant [64] based method for the approximation. The  $N$ th order cumulant is defined as

$$\kappa(\hat{Q}_1, \dots, \hat{Q}_N) = \sum_{\pi} (-1)^{|\pi|-1} (|\pi| - 1)! \prod_{B \in \pi} \left\langle \prod_{i \in B} \hat{Q}_i \right\rangle, \quad (\text{A1})$$



where  $\pi$  is the list of all partitions,  $B$  is all blocks of partition  $\pi$ , and  $|\pi|$  is the number of parts. For example, for four operators, there are four permutations with  $|\pi| = 2$  parts with the expectation value of three operators times the expectation value of one operator:  $\langle \hat{Q}_a \hat{Q}_b \hat{Q}_c \rangle \langle \hat{Q}_d \rangle$ ,  $\langle \hat{Q}_a \hat{Q}_b \hat{Q}_d \rangle \langle \hat{Q}_c \rangle$ ,  $\langle \hat{Q}_a \hat{Q}_c \hat{Q}_d \rangle \langle \hat{Q}_b \rangle$ ,  $\langle \hat{Q}_b \hat{Q}_c \hat{Q}_d \rangle \langle \hat{Q}_a \rangle$ . As another example, for four operators, there are two forms of the case with  $|\pi| = 2$ : the expectation value of three operators times the expectation value of one operator with four permutations and the expectation value of two operators times the expectation value of two operators with three permutations.

All operators in the expectation values commute in the equations above because they act on different atoms. This leads to the cumulants

$$\kappa(\hat{A}, \hat{B}) = \langle \hat{A}\hat{B} \rangle - \langle \hat{A} \rangle \langle \hat{B} \rangle, \quad (\text{A2})$$

$$\begin{aligned} \kappa(\hat{A}, \hat{B}, \hat{C}) &= \langle \hat{A}\hat{B}\hat{C} \rangle - (\langle \hat{A}\hat{B} \rangle \langle \hat{C} \rangle + \langle \hat{A}\hat{C} \rangle \langle \hat{B} \rangle \\ &\quad + \langle \hat{B}\hat{C} \rangle \langle \hat{A} \rangle) + 2\langle \hat{A} \rangle \langle \hat{B} \rangle \langle \hat{C} \rangle, \end{aligned} \quad (\text{A3})$$

$$\begin{aligned} \kappa &= \langle \hat{A}\hat{B}\hat{C}\hat{D} \rangle - (\langle \hat{A}\hat{B}\hat{C} \rangle \langle \hat{D} \rangle + 3\Pi) \\ &\quad - (\langle \hat{A}\hat{B} \rangle \langle \hat{C}\hat{D} \rangle + 2\Pi) + 2(\langle \hat{A}\hat{B} \rangle \langle \hat{C} \rangle \langle \hat{D} \rangle + 5\Pi) \\ &\quad - 6\langle \hat{A} \rangle \langle \hat{B} \rangle \langle \hat{C} \rangle \langle \hat{D} \rangle, \end{aligned} \quad (\text{A4})$$

$$\begin{aligned} \kappa &= \langle \hat{A}\hat{B}\hat{C}\hat{D}\hat{E} \rangle - (\langle \hat{A}\hat{B}\hat{C}\hat{D} \rangle \langle \hat{E} \rangle + 4\Pi) \\ &\quad - (\langle \hat{A}\hat{B}\hat{C} \rangle \langle \hat{D}\hat{E} \rangle + 9\Pi) + 2(\langle \hat{A}\hat{B}\hat{C} \rangle \langle \hat{D} \rangle \langle \hat{E} \rangle + 9\Pi) \\ &\quad + 2(\langle \hat{A}\hat{B} \rangle \langle \hat{C}\hat{D} \rangle \langle \hat{E} \rangle + 14\Pi) - 6(\langle \hat{A}\hat{B} \rangle \langle \hat{C} \rangle \langle \hat{D} \rangle \langle \hat{E} \rangle + 9\Pi) \\ &\quad + 24\langle \hat{A} \rangle \langle \hat{B} \rangle \langle \hat{C} \rangle \langle \hat{D} \rangle \langle \hat{E} \rangle, \end{aligned} \quad (\text{A5})$$

where the  $N\Pi$  in these equations indicate the  $N$  permutations with the same form as the first term in that parentheses.

## 2. Replacement of higher order expectation values

This paper truncates the order of the equations by replacing higher order operators with products of lower order operators. The prescription used is to set the cumulant to 0. The mean-field (MF1) equations arise by setting  $\kappa = 0$  in Eq. (A2), giving

$$\langle \hat{A}\hat{B} \rangle \leftarrow \langle \hat{A} \rangle \langle \hat{B} \rangle. \quad (\text{A6})$$

The MF2 equations arise by setting  $\kappa = 0$  in Eq. (A3), giving

$$\langle \hat{A}\hat{B}\hat{C} \rangle \leftarrow \langle \hat{A}\hat{B} \rangle \langle \hat{C} \rangle + \langle \hat{A}\hat{C} \rangle \langle \hat{B} \rangle + \langle \hat{B}\hat{C} \rangle \langle \hat{A} \rangle - 2\langle \hat{A} \rangle \langle \hat{B} \rangle \langle \hat{C} \rangle. \quad (\text{A7})$$

The MF3 equations arise by setting  $\kappa = 0$  in Eq. (A4), giving

$$\begin{aligned} \langle \hat{A}\hat{B}\hat{C}\hat{D} \rangle &\leftarrow (\langle \hat{A}\hat{B}\hat{C} \rangle \langle \hat{D} \rangle + 3\Pi) + (\langle \hat{A}\hat{B} \rangle \langle \hat{C}\hat{D} \rangle + 2\Pi) \\ &\quad - 2(\langle \hat{A}\hat{B} \rangle \langle \hat{C} \rangle \langle \hat{D} \rangle + 5\Pi) + 6\langle \hat{A} \rangle \langle \hat{B} \rangle \langle \hat{C} \rangle \langle \hat{D} \rangle. \end{aligned} \quad (\text{A8})$$

In the two-time formalism, the initial conditions contain expectation values for two more operators than are being propagated. For example, the MF2 initial conditions contain expectation values of four operators. Thus, Eq. (A8) cannot be directly used because it contains expectation values of three operators. For this case, we replace the expectation value of three operators with the expression in Eq. (A7). This leads to the replacement in the MF2 initial conditions,

$$\langle \hat{A}\hat{B}\hat{C}\hat{D} \rangle \leftarrow (\langle \hat{A}\hat{B} \rangle \langle \hat{C}\hat{D} \rangle + 2\Pi) - 2\langle \hat{A} \rangle \langle \hat{B} \rangle \langle \hat{C} \rangle \langle \hat{D} \rangle. \quad (\text{A9})$$

Similarly, there are expectation values of five operators in the two-time initial conditions at the MF3 level. We have not worked out the resulting equation. Instead, in our simulation, we called on the expression in Eq. (A8) when evaluating the four operator expectation value in the expression

$$\begin{aligned} \langle \hat{A}\hat{B}\hat{C}\hat{D}\hat{E} \rangle &\leftarrow (\langle \hat{A}\hat{B}\hat{C}\hat{D} \rangle \langle \hat{E} \rangle + 4\Pi) + (\langle \hat{A}\hat{B}\hat{C} \rangle \langle \hat{D}\hat{E} \rangle + 9\Pi) \\ &\quad - 2(\langle \hat{A}\hat{B}\hat{C} \rangle \langle \hat{D} \rangle \langle \hat{E} \rangle + 9\Pi) - 2(\langle \hat{A}\hat{B} \rangle \langle \hat{C}\hat{D} \rangle \langle \hat{E} \rangle \\ &\quad + 14\Pi) + 6(\langle \hat{A}\hat{B} \rangle \langle \hat{C} \rangle \langle \hat{D} \rangle \langle \hat{E} \rangle + 9\Pi) \\ &\quad + 24\langle \hat{A} \rangle \langle \hat{B} \rangle \langle \hat{C} \rangle \langle \hat{D} \rangle \langle \hat{E} \rangle. \end{aligned} \quad (\text{A10})$$

## APPENDIX B: TWO-TIME INITIAL CONDITIONS

For the two-time expectation values, the density matrix is reset due to the measurement at time  $t$ . An example case is given in Eq. (27). This leads to a reset in the values of the operators. This section gives a derivation of the new terms in the equation and the new operator values for the example in Eq. (27). The main complication is from the numerator, so this section only discusses the change in operators for a new density matrix,

$$\hat{\sigma}^- \hat{\rho}(t) \hat{\sigma}^+ \rightarrow \hat{\rho}. \quad (\text{B1})$$

All of the quantities of interest can be cast as finding the expectation value of any operator  $\hat{A}$  after the transformation in Eq. (B1). This can be written as

$$\begin{aligned} \langle \hat{A} \rangle &= \text{Tr}[\hat{A} \hat{\sigma}^- \hat{\rho}(t) \hat{\sigma}^+] = \langle \hat{\sigma}^+ \hat{A} \hat{\sigma}^- \rangle \\ &= \sum_{l,m} e^{i\varphi_{ml}} \langle \hat{\sigma}_m^+ \hat{A} \hat{\sigma}_l^- \rangle, \end{aligned} \quad (\text{B2})$$

where  $\varphi_{ml} = \vec{k} \cdot (\vec{R}_m - \vec{R}_l)$ . The complications arise when the operator  $\hat{A}$  and one of the  $\hat{\sigma}$  operators are for the same atom. For this case, the relations  $\hat{e}_n \hat{\sigma}_n^- = 0$ ,  $\hat{\sigma}_n^+ \hat{e}_n = 0$ , and  $\hat{\sigma}_n^+ \hat{\sigma}_n^- = \hat{e}_n$  are useful.

The trace of the density matrix in Eq. (B1) gives  $\langle \hat{\sigma}^+ \hat{\sigma}^- \rangle(t)$  and is obtained by setting  $\hat{A} = \hat{1}$  in Eq. (B2), giving

$$\text{Tr}[\hat{\rho}]_t = \sum_l \left[ \langle \hat{e}_l \rangle(t) + \sum'_m e^{i\varphi_{ml}} \langle \hat{\sigma}_m^+ \hat{\sigma}_l^- \rangle(t) \right], \quad (\text{B3})$$

where the prime on the sum indicates that the summation does not include identical indices, i.e.,  $m \neq l$ .

The expressions for one-atom expectation values after the transformation, given by Eq. (B1), involve two and three operator expectation values,

$$\langle \hat{\sigma}_n^- \rangle = \sum'_l [\langle \hat{\sigma}_n^- \hat{e}_l \rangle + e^{i\varphi_{nl}} \langle \hat{e}_n \hat{\sigma}_l^- \rangle + \sum'_m e^{i\varphi_{ml}} \langle \hat{\sigma}_n^- \hat{\sigma}_m^+ \hat{\sigma}_l^- \rangle], \quad (\text{B4})$$

$$\langle \hat{e}_n \rangle = \sum'_l [\langle \hat{e}_n \hat{e}_l \rangle + \sum'_m e^{i\varphi_{ml}} \langle \hat{e}_n \hat{\sigma}_m^+ \hat{\sigma}_l^- \rangle], \quad (\text{B5})$$

where the prime on a sum means the summation does not include identical indices (in each equation, the first sum has  $l \neq n$  and the second sum has  $m \neq l$  and  $m \neq n$ ). Here,  $\langle \hat{\sigma}_n^+ \rangle = \langle \hat{\sigma}_n^- \rangle^*$ .

In these equations and the ones below, the left-hand side is the expectation value for the operators after the transformation in Eq. (B1), while the right-hand side is before the transformation. This can be thought of as obtaining the expectation value at time  $t$  after the measurement, whereas those on the right-hand side are at time  $t$  before the measurement. For simplicity of notation, the  $(t)$  is dropped from this and the following equations.

The expressions for the two-atom expectation values are only for  $n \neq o$  and involve three and four operator expressions:

$$\langle \hat{\sigma}_n^- \hat{\sigma}_o^- \rangle = \sum_l' [(\hat{\sigma}_n^- \hat{\sigma}_o^- \hat{e}_l) + e^{i\varphi_{nl}} \langle \hat{e}_n \hat{\sigma}_o^- \hat{\sigma}_l^- \rangle + e^{i\varphi_{ol}} \langle \hat{\sigma}_n^- \hat{e}_o \hat{\sigma}_l^- \rangle + \sum_m' e^{i\varphi_{ml}} \langle \hat{\sigma}_n^- \hat{\sigma}_o^- \hat{\sigma}_m^+ \hat{\sigma}_l^- \rangle], \quad (\text{B6})$$

$$\langle \hat{\sigma}_n^- \hat{e}_o \rangle = \sum_l' [(\hat{\sigma}_n^- \hat{e}_o \hat{e}_l) + e^{i\varphi_{nl}} \langle \hat{e}_n \hat{e}_o \hat{\sigma}_l^- \rangle + \sum_m' e^{i\varphi_{ml}} \langle \hat{\sigma}_n^- \hat{e}_o \hat{\sigma}_m^+ \hat{\sigma}_l^- \rangle], \quad (\text{B7})$$

$$\langle \hat{e}_n \hat{e}_o \rangle = \sum_l' [(\hat{e}_n \hat{e}_o \hat{e}_l) + \sum_m' e^{i\varphi_{ml}} \langle \hat{e}_n \hat{e}_o \hat{\sigma}_m^+ \hat{\sigma}_l^- \rangle], \quad (\text{B8})$$

$$\langle \hat{\sigma}_n^- \hat{\sigma}_o^+ \rangle = e^{i\varphi_{no}} \langle \hat{e}_n \hat{e}_o \rangle + \sum_l' [(\hat{\sigma}_n^- \hat{\sigma}_o^+ \hat{e}_l) + e^{i\varphi_{nl}} \langle \hat{e}_n \hat{\sigma}_o^+ \hat{\sigma}_l^- \rangle + e^{i\varphi_{lo}} \langle \hat{\sigma}_n^- \hat{e}_o \hat{\sigma}_l^+ \rangle + \sum_m' e^{i\varphi_{ml}} \langle \hat{\sigma}_n^- \hat{\sigma}_o^+ \hat{\sigma}_m^+ \hat{\sigma}_l^- \rangle], \quad (\text{B9})$$

where the prime on a sum means that the summation does not include identical indices (in each equation, the first sum has  $l \neq n, o$  and the second sum has  $m \neq n, o, l$ ). All other expectation values can be obtained by complex conjugating these (e.g.,  $\langle \hat{\sigma}_n^+ \hat{e}_m \rangle = \langle \hat{\sigma}_n^- \hat{e}_m \rangle^*$ ). While these equations look complicated, the expressions come from the straightforward application of Eq. (B2). For example, in Eq. (B6), the first term arises when  $m = l$  but  $l \neq n$  or  $o$ , the second term is when  $m = n$  but  $l \neq n$  or  $o$ , the third term is when  $m = o$  but  $l \neq n$  or  $o$ , and the last term is when none of the indices are the same.

The expressions for the three-atom expectation values are only for the case where none of  $n, o, p$  are the same and

involve four and five operator expressions:

$$\langle \hat{\sigma}_n^- \hat{\sigma}_o^- \hat{\sigma}_p^- \rangle = \sum_l' [(\hat{\sigma}_n^- \hat{\sigma}_o^- \hat{\sigma}_p^- \hat{e}_l) + e^{i\varphi_{nl}} \langle \hat{e}_n \hat{\sigma}_o^- \hat{\sigma}_p^- \hat{\sigma}_l^- \rangle + e^{i\varphi_{ol}} \langle \hat{\sigma}_n^- \hat{e}_o \hat{\sigma}_p^- \hat{\sigma}_l^- \rangle + e^{i\varphi_{pl}} \langle \hat{\sigma}_n^- \hat{\sigma}_o^- \hat{e}_p \hat{\sigma}_l^- \rangle + \sum_m' e^{i\varphi_{ml}} \langle \hat{\sigma}_n^- \hat{\sigma}_o^- \hat{\sigma}_p^- \hat{\sigma}_m^+ \hat{\sigma}_l^- \rangle], \quad (\text{B10})$$

$$\langle \hat{\sigma}_n^- \hat{\sigma}_o^- \hat{e}_p \rangle = \sum_l' [(\hat{\sigma}_n^- \hat{\sigma}_o^- \hat{e}_p \hat{e}_l) + e^{i\varphi_{nl}} \langle \hat{e}_n \hat{\sigma}_o^- \hat{e}_p \hat{\sigma}_l^- \rangle + e^{i\varphi_{ol}} \langle \hat{\sigma}_n^- \hat{e}_o \hat{e}_p \hat{\sigma}_l^- \rangle + \sum_m' e^{i\varphi_{ml}} \langle \hat{\sigma}_n^- \hat{\sigma}_o^- \hat{e}_p \hat{\sigma}_m^+ \hat{\sigma}_l^- \rangle], \quad (\text{B11})$$

$$\langle \hat{\sigma}_n^- \hat{e}_o \hat{e}_p \rangle = \sum_l' [(\hat{\sigma}_n^- \hat{e}_o \hat{e}_p \hat{e}_l) + e^{i\varphi_{nl}} \langle \hat{e}_n \hat{e}_o \hat{e}_p \hat{\sigma}_l^- \rangle + \sum_m' e^{i\varphi_{ml}} \langle \hat{\sigma}_n^- \hat{e}_o \hat{e}_p \hat{\sigma}_m^+ \hat{\sigma}_l^- \rangle], \quad (\text{B12})$$

$$\langle \hat{e}_n \hat{e}_o \hat{e}_p \rangle = \sum_l' [(\hat{e}_n \hat{e}_o \hat{e}_p \hat{e}_l) + \sum_m' e^{i\varphi_{ml}} \langle \hat{e}_n \hat{e}_o \hat{e}_p \hat{\sigma}_m^+ \hat{\sigma}_l^- \rangle], \quad (\text{B13})$$

$$\langle \hat{\sigma}_n^- \hat{\sigma}_o^- \hat{\sigma}_p^+ \rangle = e^{i\varphi_{np}} \langle \hat{e}_n \hat{\sigma}_o^- \hat{e}_p \rangle + e^{i\varphi_{op}} \langle \hat{\sigma}_n^- \hat{e}_o \hat{e}_p \rangle + \sum_l' [(\hat{\sigma}_n^- \hat{\sigma}_o^- \hat{\sigma}_p^+ \hat{e}_l) + e^{i\varphi_{nl}} \langle \hat{e}_n \hat{\sigma}_o^- \hat{\sigma}_p^+ \hat{\sigma}_l^- \rangle + e^{i\varphi_{ol}} \langle \hat{\sigma}_n^- \hat{e}_o \hat{\sigma}_p^+ \hat{\sigma}_l^- \rangle + e^{-i\varphi_{pl}} \langle \hat{\sigma}_n^- \hat{\sigma}_o^- \hat{e}_p \hat{\sigma}_l^+ \rangle + \sum_m' e^{i\varphi_{ml}} \langle \hat{\sigma}_n^- \hat{\sigma}_o^- \hat{\sigma}_p^+ \hat{\sigma}_m^+ \hat{\sigma}_l^- \rangle], \quad (\text{B14})$$

$$\langle \hat{\sigma}_n^- \hat{e}_o \hat{\sigma}_p^+ \rangle = e^{i\varphi_{np}} \langle \hat{e}_n \hat{e}_o \hat{e}_p \rangle + \sum_l' [(\hat{\sigma}_n^- \hat{e}_o \hat{\sigma}_p^+ \hat{e}_l) + e^{i\varphi_{nl}} \langle \hat{e}_n \hat{e}_o \hat{\sigma}_p^+ \hat{\sigma}_l^- \rangle + e^{-i\varphi_{pl}} \langle \hat{\sigma}_n^- \hat{e}_o \hat{e}_p \hat{\sigma}_l^+ \rangle + \sum_m' e^{i\varphi_{ml}} \langle \hat{\sigma}_n^- \hat{e}_o \hat{\sigma}_p^+ \hat{\sigma}_m^+ \hat{\sigma}_l^- \rangle], \quad (\text{B15})$$

where the prime on a sum means the summation does not include identical indices (in each equation, the first sum has  $l \neq n, o, p$  and the second sum has  $m \neq n, o, p, l$ ). All other expectation values can be obtained by complex conjugating these.

- [1] R. H. Dicke, Coherence in spontaneous radiation processes, *Phys. Rev.* **93**, 99 (1954).
- [2] N. E. Rehler and J. H. Eberly, Superradiance, *Phys. Rev. A* **3**, 1735 (1971).
- [3] M. Gross and S. Haroche, Superradiance: An essay on the theory of collective spontaneous emission, *Phys. Rep.* **93**, 301 (1982).
- [4] M. O. Scully, E. S. Fry, C. H. Raymond Ooi, and K. Wódkiewicz, Directed Spontaneous Emission from an Extended Ensemble of  $n$  Atoms: Timing is Everything, *Phys. Rev. Lett.* **96**, 010501 (2006).

- [5] A. A. Svidzinsky, J.-T. Chang, and M. O. Scully, Dynamical Evolution of Correlated Spontaneous Emission of a Single Photon from a Uniformly Excited Cloud of  $n$  Atoms, *Phys. Rev. Lett.* **100**, 160504 (2008).
- [6] A. Svidzinsky and J.-T. Chang, Cooperative spontaneous emission as a many-body eigenvalue problem, *Phys. Rev. A* **77**, 043833 (2008).
- [7] A. S. Kuraptsev and I. M. Sokolov, Spontaneous decay of an atom excited in a dense and disordered atomic ensemble: Quantum microscopic approach, *Phys. Rev. A* **90**, 012511 (2014).

- [8] F. Cottier, R. Kaiser, and R. Bachelard, Role of disorder in super- and subradiance of cold atomic clouds, *Phys. Rev. A* **98**, 013622 (2018).
- [9] M. Chalony, R. Pierrat, D. Delande, and D. Wilkowski, Coherent flash of light emitted by a cold atomic cloud, *Phys. Rev. A* **84**, 011401(R) (2011).
- [10] G.-D. Lin and S. F. Yelin, Superradiance in spin- $j$  particles: Effects of multiple levels, *Phys. Rev. A* **85**, 033831 (2012).
- [11] T. Bienaimé, N. Piovella, and R. Kaiser, Controlled Dicke Subradiance from a Large Cloud of Two-Level Systems, *Phys. Rev. Lett.* **108**, 123602 (2012).
- [12] D. D. Yavuz, Superradiance as a source of collective decoherence in quantum computers, *J. Opt. Soc. Am. B* **31**, 2665 (2014).
- [13] W. Guerin, M. O. Araújo, and R. Kaiser, Subradiance in a Large Cloud of Cold Atoms, *Phys. Rev. Lett.* **116**, 083601 (2016).
- [14] R. T. Sutherland and F. Robicheaux, Superradiance in inverted multilevel atomic clouds, *Phys. Rev. A* **95**, 033839 (2017).
- [15] L. Ostermann, C. Meignant, C. Genes, and H. Ritsch, Super- and subradiance of clock atoms in multimode optical waveguides, *New J. Phys.* **21**, 025004 (2019).
- [16] A. Asenjo-Garcia, M. Moreno-Cardoner, A. Albrecht, H. J. Kimble, and D. E. Chang, Exponential Improvement in Photon Storage Fidelities Using Subradiance and Selective Radiance in Atomic Arrays, *Phys. Rev. X* **7**, 031024 (2017).
- [17] Y.-X. Zhang and K. Mølmer, Theory of Subradiant States of a One-Dimensional Two-Level Atom Chain, *Phys. Rev. Lett.* **122**, 203605 (2019).
- [18] P.-O. Guimond, A. Grankin, D. V. Vasilyev, B. Vermersch, and P. Zoller, Subradiant Bell States in Distant Atomic Arrays, *Phys. Rev. Lett.* **122**, 093601 (2019).
- [19] J. A. Needham, I. Lesanovsky, and B. Olmos, Subradiance-protected excitation transport, *New J. Phys.* **21**, 073061 (2019).
- [20] S. J. Masson, I. Ferrier-Barbut, L. A. Orozco, A. Browaeys, and A. Asenjo-Garcia, Many-Body Signatures of Collective Decay in Atomic Chains, *Phys. Rev. Lett.* **125**, 263601 (2020).
- [21] J. Rui, D. Wei, A. Rubio-Abadal, S. Hollerith, J. Zeiher, D. M. Stamper-Kurn, C. Gross, and I. Bloch, A subradiant optical mirror formed by a single structured atomic layer, *Nature (London)* **583**, 369 (2020).
- [22] D. E. Chang, J. Ye, and M. D. Lukin, Controlling dipole-dipole frequency shifts in a lattice-based optical atomic clock, *Phys. Rev. A* **69**, 023810 (2004).
- [23] Z. Meir, O. Schwartz, E. Shahmoon, D. Oron, and R. Ozeri, Cooperative Lamb Shift in a Mesoscopic Atomic Array, *Phys. Rev. Lett.* **113**, 193002 (2014).
- [24] A. Cidrim, T. S. do Espirito Santo, J. Schachenmayer, R. Kaiser, and R. Bachelard, Photon Blockade with Ground-State Neutral Atoms, *Phys. Rev. Lett.* **125**, 073601 (2020).
- [25] R. Friedberg, S. R. Hartmann, and J. T. Manassah, Frequency shifts in emission and absorption by resonant systems of two-level atoms, *Phys. Rep.* **7**, 101 (1973).
- [26] A. A. Svidzinsky, J.-T. Chang, and M. O. Scully, Cooperative spontaneous emission of  $n$  atoms: Many-body eigenstates, the effect of virtual Lamb shift processes, and analogy with radiation of  $n$  classical oscillators, *Phys. Rev. A* **81**, 053821 (2010).
- [27] T. Ido, T. H. Loftus, M. M. Boyd, A. D. Ludlow, K. W. Holman, and J. Ye, Precision Spectroscopy and Density-Dependent Frequency Shifts in Ultracold Sr, *Phys. Rev. Lett.* **94**, 153001 (2005).
- [28] J. Keaveney, A. Sargsyan, U. Krohn, I. G. Hughes, D. Sarkisyan, and C. S. Adams, Cooperative Lamb Shift in an Atomic Vapor Layer of Nanometer Thickness, *Phys. Rev. Lett.* **108**, 173601 (2012).
- [29] J. Javanainen, J. Ruostekoski, Y. Li, and S.-M. Yoo, Shifts of a resonance line in a dense atomic sample, *Phys. Rev. Lett.* **112**, 113603 (2014).
- [30] A. Glicenstein, G. Ferioli, N. Šibalić, L. Brossard, I. Ferrier-Barbut, and A. Browaeys, Collective Shift in Resonant Light Scattering by a One-Dimensional Atomic Chain, *Phys. Rev. Lett.* **124**, 253602 (2020).
- [31] J. Javanainen and J. Ruostekoski, Light propagation beyond the mean-field theory of standard optics, *Opt. Express* **24**, 993 (2016).
- [32] P. W. Courteille, S. Bux, E. Lucioni, K. Lauber, T. Bienaime, R. Kaiser, and N. Piovella, Modification of radiation pressure due to cooperative scattering of light, *The Eur. Phys. J. D* **58**, 69 (2010).
- [33] M.-T. Rouabah, M. Samoylova, R. Bachelard, P. W. Courteille, R. Kaiser, and N. Piovella, Coherence effects in scattering order expansion of light by atomic clouds, *J. Opt. Soc. Am. A* **31**, 1031 (2014).
- [34] J. Pellegrino, R. Bourgain, S. Jennewein, Y. R. P. Sortais, A. Browaeys, S. D. Jenkins, and J. Ruostekoski, Observation of Suppression of Light Scattering Induced by Dipole-Dipole Interactions in a Cold-Atom Ensemble, *Phys. Rev. Lett.* **113**, 133602 (2014).
- [35] S. L. Bromley, B. Zhu, M. Bishof, X. Zhang, T. Bothwell, J. Schachenmayer, T. L. Nicholson, R. Kaiser, S. F. Yelin, M. D. Lukin, A. M. Rey, and J. Ye, Collective atomic scattering and motional effects in a dense coherent medium, *Nat. Commun.* **7**, 1 (2016).
- [36] S. Jennewein, M. Besbes, N. J. Schilder, S. D. Jenkins, C. Sauvan, J. Ruostekoski, J.-J. Greffet, Y. R. P. Sortais, and A. Browaeys, Coherent Scattering of Near-Resonant Light by a Dense Microscopic Cold Atomic Cloud, *Phys. Rev. Lett.* **116**, 233601 (2016).
- [37] B. Zhu, J. Cooper, J. Ye, and A. M. Rey, Light scattering from dense cold atomic media, *Phys. Rev. A* **94**, 023612 (2016).
- [38] F. Robicheaux and R. T. Sutherland, Photon scattering from a cold, Gaussian atom cloud, *Phys. Rev. A* **101**, 013805 (2020).
- [39] E. Shahmoon, D. S. Wild, M. D. Lukin, and S. F. Yelin, Cooperative Resonances in Light Scattering from Two-Dimensional Atomic Arrays, *Phys. Rev. Lett.* **118**, 113601 (2017).
- [40] S. D. Jenkins and J. Ruostekoski, Controlled manipulation of light by cooperative response of atoms in an optical lattice, *Phys. Rev. A* **86**, 031602(R) (2012).
- [41] R. J. Bettles, S. A. Gardiner, and C. S. Adams, Enhanced Optical Cross Section via Collective Coupling of Atomic Dipoles in a 2D Array, *Phys. Rev. Lett.* **116**, 103602 (2016).
- [42] A. Grankin, P.-O. Guimond, D. V. Vasilyev, B. Vermersch, and P. Zoller, Free-space photonic quantum link and chiral quantum optics, *Phys. Rev. A* **98**, 043825 (2018).
- [43] R. T. Sutherland and F. Robicheaux, Collective dipole-dipole interactions in an atomic array, *Phys. Rev. A* **94**, 013847 (2016).
- [44] C. Qu and A. M. Rey, Spin squeezing and many-body dipolar dynamics in optical lattice clocks, *Phys. Rev. A* **100**, 041602 (2019).

- [45] A. Asenjo-Garcia, H. J. Kimble, and D. E. Chang, Optical waveguiding by atomic entanglement in multilevel atom arrays, *Proc. Natl. Acad. Sci.* **116**, 25503 (2019).
- [46] L. Henriot, J. S. Douglas, D. E. Chang, and A. Albrecht, Critical open-system dynamics in a one-dimensional optical-lattice clock, *Phys. Rev. A* **99**, 023802 (2019).
- [47] L. A. Williamson, M. O. Borgh, and J. Ruostekoski, Superatom Picture of Collective Nonclassical Light Emission and Dipole Blockade in Atom Arrays, *Phys. Rev. Lett.* **125**, 073602 (2020).
- [48] L. A. Williamson and J. Ruostekoski, Optical response of atom chains beyond the limit of low light intensity: The validity of the linear classical oscillator model, *Phys. Rev. Research* **2**, 023273 (2020).
- [49] R. J. Bettles, M. D. Lee, S. A. Gardiner, and J. Ruostekoski, Quantum and nonlinear effects in light transmitted through planar atomic arrays, *Commun. Phys.* **3**, 141 (2020).
- [50] J. Javanainen, J. Ruostekoski, Y. Li, and S.-M. Yoo, Exact electrodynamics versus standard optics for a slab of cold dense gas, *Phys. Rev. A* **96**, 033835 (2017).
- [51] T. S. do Espirito Santo, P. Weiss, A. Cipris, R. Kaiser, W. Guerin, R. Bachelard, and J. Schachenmayer, Collective excitation dynamics of a cold atom cloud, *Phys. Rev. A* **101**, 013617 (2020).
- [52] S. E. Skipetrov and I. M. Sokolov, Magnetic-Field-Driven Localization of Light in a Cold-Atom Gas, *Phys. Rev. Lett.* **114**, 053902 (2015).
- [53] R. T. Sutherland and F. Robicheaux, Coherent forward broadening in cold atom clouds, *Phys. Rev. A* **93**, 023407 (2016).
- [54] J. Ruostekoski and J. Javanainen, Quantum field theory of cooperative atom response: Low light intensity, *Phys. Rev. A* **55**, 513 (1997).
- [55] S. Krämer and H. Ritsch, Generalized mean-field approach to simulate the dynamics of large open spin ensembles with long range interactions, *Eur. Phys. J. D* **69**, 282 (2015).
- [56] M. Fleischhauer and S. F. Yelin, Radiative atom-atom interactions in optically dense media: Quantum corrections to the Lorentz-Lorenz formula, *Phys. Rev. A* **59**, 2427 (1999).
- [57] C. Hotter, D. Plankensteiner, and H. Ritsch, Continuous narrowband lasing with coherently driven v-level atoms, *New J. Phys.* **22**, 113021 (2020).
- [58] P. Kirton and J. Keeling, Superradiant and lasing states in driven-dissipative Dicke models, *New J. Phys.* **20**, 015009 (2018).
- [59] P. Kirton, M. M. Roses, J. Keeling, and E. G. Dalla Torre, Introduction to the Dicke model: From equilibrium to nonequilibrium, and vice versa, *Adv. Quantum Technol.* **2**, 1800043 (2019).
- [60] M. Sánchez-Barquilla, R. E. F. Silva, and J. Feist, Cumulant expansion for the treatment of light-matter interactions in arbitrary material structures, *J. Chem. Phys.* **152**, 034108 (2020).
- [61] R. Loudon, *The Quantum Theory of Light*, 3rd ed. (Oxford University Press, New York, 2000).
- [62] R. Jones, R. Saint, and B. Olmos, Far-field resonance fluorescence from a dipole-interacting laser-driven cold atomic gas, *J. Phys. B.* **50**, 014004 (2016).
- [63] J. D. Jackson, *Classical Electrodynamics*, 3rd ed. (Wiley, New York, 1999).
- [64] R. Kubo, Generalized cumulant expansion method, *J. Phys. Soc. Jpn.* **17**, 1100 (1962).
- [65] This follows the notation in Ref. [48]. The normalization  $\sum_n u_\alpha(\vec{R}_n)u_{\alpha'}(\vec{R}_n) = 1$  for complex symmetric matrices could have been chosen.
- [66] A. Piñeiro Orioli, A. Safavi-Naini, M. L. Wall, and A. M. Rey, Nonequilibrium dynamics of spin-boson models from phase-space methods, *Phys. Rev. A* **96**, 033607 (2017).
- [67] S. Czischek, M. Gärttner, M. Oberthaler, M. Kastner, and T. Gasenzer, Quenches near criticality of the quantum Ising chain—power and limitations of the discrete truncated Wigner approximation, *Quantum Sci. Technol.* **4**, 014006 (2018).
- [68] D. Plankensteiner, C. Hotter, and H. Ritsch, Quantumcumulants.jl: A julia framework for generalized mean-field equations in open quantum systems, [arXiv:2105.01657](https://arxiv.org/abs/2105.01657).